Available online at www.sciencedirect.com
SCIENCE DIRECT®
Journal of Power Sources 135 (2004) 135–151
JOURNAL OF POWER SOURCES
www.elsevier.com/locate/jpowsour

Model-based control of fuel cells: (1) Regulatory control

Joshua Golbert, Daniel R. Lewin*

PSE Research Group, Wolfson Department of Chemical Engineering, Technion I.I.T., Haifa 32000, Israel

Received 24 October 2003; received in revised form 5 April 2004; accepted 17 April 2004

Available online 28 July 2004

Abstract

This paper describes a model-based controller for the regulation of a proton exchange membrane (PEM) fuel cell. The model accounts for spatial dependencies of voltage, current, material flows, and temperatures in the fuel channel. Analysis of the process model shows that the effective gain of the process undergoes a sign change in the normal operating range of the fuel cell, indicating that it cannot be stabilized using a linear controller with integral action. Consequently, a nonlinear model-predictive-controller based on a simplified model has been developed, enabling the use of optimal control to satisfy power demands robustly. The models and controller have been realized in the MATLAB and SIMULINK environment. Initial results indicate improved performance and robustness when using model-based control in comparison with that obtained using an adaptive controller.

Keywords: PEM fuel cell dynamics; Model-based control; Model predictive control; Transient model

1. Introduction

Fuel cells are chemical engines that convert chemical potential into electrical power. Since they are not based on temperature differences, they are not subjected to Carnot's limit of efficiency. In addition, common pollutants such as sulfur dioxide and nitrous oxides are avoided since the process does not involve combustion. These advantages, together with the reduction of greenhouse gases and fuel consumption due to higher efficiencies and the possibility of alternative energy sources, have generated enormous interest in fuel cells for stationary as well as mobile applications.

The heart of the fuel cell system consists of two electrodes: the anode and cathode. The most basic system uses pure hydrogen as fuel, which is oxidized at the anode, producing electrons and protons. The electrons are released to an external circuit, where they can be used to perform work, while the protons diffuse through a membrane to the cathode. At the cathode, oxygen reacts with the electrons from the external circuit and protons from the anode reaction, forming water. Other systems are being developed, including the use of methanol as fuel (fed directly to the fuel cell [10], or reformed externally to produce hydrogen) and even using traditional fossil fuels. Whatever the actual configuration, the basic principles remain the same.

The dynamics of fuel cells are complex and include the mass transport of materials through the membrane and to and from the electrodes, reaction mechanisms and rates at the electrodes, voltages and currents produced depending on the pressures, temperatures and concentrations at the electrodes, overpotential and Ohmic losses of voltage throughout the process. Several alternative models of different complexity have been proposed to describe the performance of fuel cells under an array of conditions (e.g., [4,12,8]). These models are then used to evaluate optimal schemes of external heating, water management [5] and fuel composition.

The dynamic response of fuel cells is important for vehicular applications, where power demands fluctuate, and the fuel cell does not usually operate at the optimal steady-state designed by the fuel cell manufacturer. A empirical model for the transient response of a fuel cell was developed by [1]. However, this model is lumped and therefore does not accurately portray the spatial dependencies in the system. In a similar fashion Kang et al. [7] present an analysis of a dynamic model for a molten-carbonate fuel cell (MCFC), where the system is modeled as a collection of first order transfer functions with dead times. Pukrushpan et al. [9] present a nonlinear, zero-dimensional, dynamic model of a fuel cell, but this model is also empirical.

* Corresponding author. Tel.: +972 4 8292 006; fax: +972 4 8295 672.
E-mail address: dlewin@tx.technion.ac.il (D.R. Lewin).
URL: http://tx.technion.ac.il/~dlewin/pse.htm.

0378-7753/$ – see front matter © 2004 Elsevier B.V. All rights reserved.
doi:10.1016/j.jpowsour.2004.04.008

Nomenclature

A	heat exchange area per unit length (cm)
a	water activity
c	concentration at membrane surface (mol/cm^3)
C_p	mass heat capacity (J/(g K))
d	channel height (cm)
D	diffusion coefficient in diffusion layer (cm^2/s)
D_0	intradiffusion coefficient of water in membrane (cm^2/s)
D^*	diffusion coefficient of water in membrane (cm^2/s)
e	membrane area per unit length (cm)
f	cross-section of solid (cm^2)
F	Faraday's constant (Col/equivalent)
h	channel width (cm)
I	current density (A/cm^2)
I_0	exchange current density (A/cm^2)
k	heat conduction coefficient (W/(cm K))
k_c	condensation rate constant (s^{-1})
k_p	water permeability (cm^2)
L	channel length (cm)
M	molar flow (mol/s)
$W_{m,dry}$	membrane dry weight (g/mol)
n_d	electro-osmotic coefficient of water in membrane (molecules/protons)
P	pressure (atm)
T	temperature (K)
t_m	membrane thickness (cm)
U	convective heat transfer coefficient (W/(cm^2 K))
V	voltage (V)

Greek symbols

μ	Water viscosity (g/(cm s))
α	Ratio of water molecules per proton flux (molecules/protons)
δ	Diffusion layer thickness (cm)
ΔH	Enthalpy of overall reaction (J/mol)
ΔH_{vap}	Enthalpy of water evaporation (J/mol)
ρ	Density (g/cm^3)
$\rho_{m,dry}$	Dry membrane density (g/cm^3)
σ	Membrane conductivity (Ohm^{-1} cm^{-1})

Subscript

a	Anode
avg	Average
c	Cathode
cool	Coolant
g	Gas
H_2	Hydrogen
in	Inlet
inf	Surroundings
N_2	Nitrogen
O_2	Oxygen
oc	Open circuit
s	Solid
set	Set point
w	Water

Superscript

l	Liquid
sat	Saturation
v	Vapor

This paper focuses on the crucial issue of how to control the fuel cell to ensure acceptable response time for the power demand, while achieving high efficiencies over the entire operating range. To assist in addressing this issue, Section 2 presents a spatial, time-dependent model of a fuel cell. The analysis of fuel-cell controllability follows, relying on the developed model, as well as the synthesis of an adaptive controller, intended to account for the observed sign-change in the process static gain. Section 3 describes an alternative approach, relying on a reduced-order model, and the use of the model in a robust model predictive control (MPC) scheme, which satisfies the power demand over a wide range of conditions, and is demonstrated to provide performance superior to that of the adaptive scheme.

2. Model formulation and solution

The model is based on the concept presented by [12], where a fuel cell is modeled along its channel, as shown in Fig. 1. The model accounts for heat transfer between the solid and the two gas channels, and between the solid and cooling water. The water content is modeled, as well,

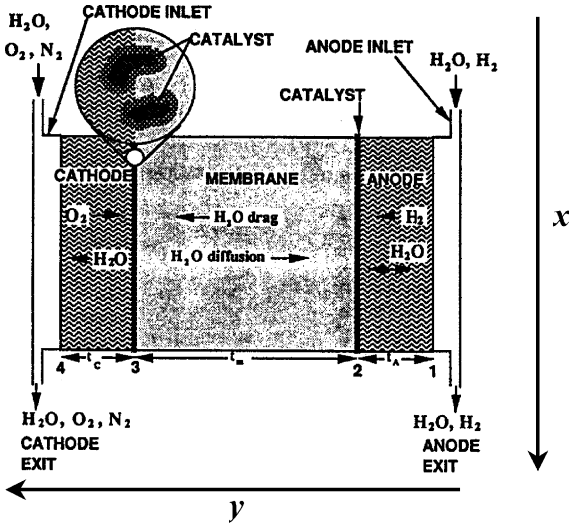

Fig. 1. Schematic diagram of fuel cell channel.

calculating the condensation and evaporation, water drag through the membrane, and water generation at the cathode. The energy balance on the solid is modeled dynamically whereas all the other equations are assumed to be at quasi-steady-state for a given solid temperature profile. Other equations vary slightly from those presented by Yi and Nguyen, as well. Namely, the heat generation term is taken from Berger [3], since this term can be easily expressed in terms of temperature (although this has not been carried out in the present study).

The dynamics of the electrochemistry, as well as the transient response of the fluids in the channels (anode cathode and coolant), are assumed to be instantaneous relative to the thermal transient response of the solid. Consequently, conservation equations that model the entire system, with the exception of the fuel cell solid support, are formulated in quasi-steady-state [1]. This greatly reduces the complexity of the system since it is reduced to a one-dimensional problem.For a given local current density (A/cm^2), the reactants are consumed as follows

$$\frac{\mathrm{d}M_{\mathrm{H_2}}(x)}{\mathrm{d}x} = -\frac{h}{2F} I(x) \tag{1}$$

$$\frac{\mathrm{d}M_{\mathrm{O_2}}(x)}{\mathrm{d}x} = -\frac{h}{4F} I(x) \tag{2}$$

The change in the flow rate of liquid water in each flow channel, which is influenced solely by evaporation and condensation, is given as

$$\frac{\mathrm{d}M^{\mathrm{l}}_{\mathrm{w},k}(x)}{\mathrm{d}x} = \frac{k_{\mathrm{c}} h d}{RT_k(x)} \left\{ \frac{M^{\mathrm{v}}_{\mathrm{w},k}(x)}{\sum_i^{N_{\mathrm{k}}} M_{i,k}(x)} P_k - P^{\mathrm{sat}}_{\mathrm{w}}(T_k) \right\}, \quad k = \mathrm{a}, \mathrm{c} \tag{3}$$

This implies that the rate of condensation/evaporation is proportional to the difference between the partial pressure of water and the saturation pressure at the local temperature. Note that in the event of no liquid water and a partial pressure lower than the saturation pressure, this equation is not valid. (See Appendix C on how this is dealt with during integration). The water vapor in the flow channels is affected by a number of mechanisms: (a) water vapor is generated at the cathode by the reaction of oxygen with the proton and electron; (b) water vapor diffuses through the membrane; (c) water vapor is dragged through the membrane by migrating protons (from the anode to the cathode); (d) liquid water can condense and evaporate based on the partial pressure of water and the saturated pressure (temperature-dependent). These mechanisms are included in the following equation, which models the anode flow channel

$$\frac{\mathrm{d}M^{\mathrm{v}}_{\mathrm{w,a}}(x)}{\mathrm{d}x} = -\frac{\mathrm{d}M^{\mathrm{l}}_{\mathrm{w,a}}(x)}{\mathrm{d}x} - \frac{h\alpha(x)}{F} I(x), \tag{4}$$

where the first term on the right is the condensation or evaporation of the water and the second is the net migration of water across the membrane. This net migration is the combined effect of diffusion by concentration and pressure gradients along the membrane and water molecules dragged across the membrane by the current. The ratio of water molecules per proton, α, is given by

$$\begin{aligned}\alpha &= n_{\mathrm{d}} - \frac{F}{I(x)} D^* \frac{\mathrm{d}c_{\mathrm{w}}}{\mathrm{d}y} - c_{\mathrm{w}} \frac{k_{\mathrm{p}}}{\mu} \frac{F}{I(x)} \frac{\mathrm{d}P_{\mathrm{w}}}{\mathrm{d}y} \\ &\approx n_{\mathrm{d}} - \frac{F}{I(x)} D^* \frac{c_{\mathrm{w,c}} - c_{\mathrm{w,a}}}{t_{\mathrm{m}}} \\ &\quad - \frac{(c_{\mathrm{w,a}} + c_{\mathrm{w,c}})}{2} \frac{k_{\mathrm{p}}}{\mu} \frac{F}{I(x)} \frac{P_{\mathrm{w,c}} - P_{\mathrm{w,a}}}{t_{\mathrm{m}}}\end{aligned} \tag{5}$$

The water vapor content of the cathode is modeled using the following equation, which includes the generation of water by reaction

$$\frac{\mathrm{d}M^{\mathrm{v}}_{\mathrm{w,c}}(x)}{\mathrm{d}x} = -\frac{\mathrm{d}M^{\mathrm{l}}_{\mathrm{w,c}}(x)}{\mathrm{d}x} + \frac{h}{2F} I(x) + \frac{h\alpha(x)}{F} I(x) \tag{6}$$

The local temperatures in the anode, cathode and coolant channels are affected by heat transfer between the mass surface and the fluid

$$\frac{\mathrm{d}T_k(x)}{\mathrm{d}x} = \frac{U_{\mathrm{g}} A_{\mathrm{g}} \{T_{\mathrm{s}}(x) - T_k(x)\}}{\sum_i C_{\mathrm{p},i} M_i(x)}, \quad k = \mathrm{a}, \mathrm{c} \tag{7}$$

$$\frac{\mathrm{d}T_{\mathrm{cool}}(x)}{\mathrm{d}x} = \frac{U_{\mathrm{cool}} A_{\mathrm{cool}} \{T_{\mathrm{s}}(x) - T_{\mathrm{cool}}(x)\}}{C_{\mathrm{p,w}} M_{\mathrm{cool}}} \tag{8}$$

The cell voltage is inversely proportional to the current density, and related to the partial pressures of the species, using the Nernst and Tafel equations [2]

$$V_{\mathrm{cell}} = V_{\mathrm{oc}} + \frac{RT}{2F} \ln \left(\frac{\left[P_{\mathrm{H_2,b}}(x) - \left(\frac{\delta I(x)}{2FD_{\mathrm{H_2}}} \right) \right] \times \left[P_{\mathrm{O_2,b}}(x) - \left(\frac{\delta I(x)}{4FD_{\mathrm{O_2}}} \right) \right]^{0.5}}{P_{\mathrm{H_2O,b}}(x) + \left(\frac{\delta I(x)}{2FD_{\mathrm{H_2O}}} \right)} \right) - \frac{RT}{F} \ln \left(\frac{I(x)}{I_0 \left(P_{\mathrm{O_2,b}}(x) - \frac{\delta I(x)}{4FD_{\mathrm{O_2}}} \right)} \right) - \frac{I(x) t_{\mathrm{m}}}{\sigma_{\mathrm{m}}(x)} \tag{9}$$

This equation is derived as shown in Appendix A. Thus, the effective cell voltage is the thermodynamically reversible cell voltage minus the Ohmic, activation and concentration overpotentials. The partial pressures are simply the molar ratios multiplied by the electrode pressure

$$P_{\mathrm{i}} = \frac{M_{\mathrm{i}}}{\sum M_{\mathrm{j}}} P \tag{10}$$

The following are empirical expressions of the various constants used in the model equations (following [11])

$$\sigma_{\mathrm{m}} = \left(0.00514 \frac{W_{\mathrm{m,dry}}}{\rho_{\mathrm{dry}}} c_{\mathrm{w},a} - 0.00326 \right) \exp \left(\frac{1}{303} - \frac{1}{T_{\mathrm{s}}} \right) \tag{11}$$

$$c_{w,k}=\begin{cases}\dfrac{\rho_{dry}}{W_{m,dry}}(0.043+17.8a_k-39.85a_k^2+36a_k^3) & a_k\le 1 \quad k=a,c\\ \dfrac{\rho_{dry}}{W_{m,dry}}(14+1.4(a_k-1)) & a_k>1 \quad k=a,c\end{cases} \tag{12}$$

$$a_k=\frac{M^v_{w,k}}{\sum_i C_{p,i}M_i(x)}\frac{P_k}{P_{sat}(T_k-273)},\quad k=a,c \tag{13}$$

$$P_{sat}(T)=10^{-2.18+2.95\times10^{-2}T-9.18\times10^{-5}T^2+1.44\times10^{-7}T^3} \tag{14}$$

$$n_d=\begin{cases}0.0049+2.024a_a-4.53a_a^2+4.09a_a^3 & a_a\le 1\\ 1.59+0.159(a_a-1) & a_a>1\end{cases} \tag{15}$$

$$D^*=n_dD_0\exp\left(2416\left(\frac{1}{303}-\frac{1}{T_s}\right)\right) \tag{16}$$

$$\Delta H_{vap}(T)=45,070-41.94T+3.44\times10^{-3}T^2+2.54810^{-6}T^3-8.98\times10^{-10}T^4 \tag{17}$$

The heart of the model is a spatial, time-dependent partial differential equation describing the local temperature of the solid cell support

$$\rho_sCp_s\frac{\partial T_s}{\partial t}=k_s\frac{\partial^2T_s}{\partial x^2}+\frac{U_gA_g}{f}(T_a+T_c-2T_s)+\frac{U_{cool}A_{cool}}{f}(T_{cool}-T_s)-\frac{e}{f}\left(\frac{\Delta H}{2F}+V_{cell}\right)I(x)+\frac{1}{f}\Delta H_{vap}(T)\left(\frac{dM^l_{w,a}(x)}{dx}+\frac{dM^l_{w,c}(x)}{dx}\right), \tag{18}$$

with boundary conditions

$$k\left.\frac{\partial T_s}{\partial x}\right|_{x=0}=U_c(T_s-T_{inf})$$
$$k\left.\frac{\partial T_s}{\partial x}\right|_{x=L}=-U_c(T_s-T_{inf}) \tag{19}$$

Evidently, the channel solid temperature is affected by: (1) heat transfer by conduction, (2) heat transfer by convection with the flow and coolant channels, (3) heat generation by the reaction (total enthalpy change of the reaction (water formation) minus the external power [3]) and (4) heat of condensation/evaporation of water in the flow channels. The boundary conditions, shown in Eq. (19), reflect heat losses to the surroundings from the edges. It is assumed that there is no heat loss along the channel, since the channel is part of a large, symmetrical proton exchange membrane (PEM) stack.

2.1. Solution procedure

Eq. (18) is integrated using the Crank–Nicholson method, in which the partial differential equation is discretized, resulting in a system of algebraic equations that defines the dependence between the solid temperature profiles for consecutive times. For each time-step in the integration, the quasi-steady state ODEs (Eqs. (1)–(8)) are integrated, and the surface temperature profile is calculated for the next time-step. Full details of the Crank–Nicholson method and calculations are presented in Appendix D.

During the integration of the ODEs the cell voltage is set. If the system is modeled for constant voltage, the average current density is calculated for every time step of the Crank–Nicholson integration by integrating the values of $I(x)$ over x and dividing by the length of the channel. However, if the system has a set current density, the voltage is guessed and iteratively manipulated (using the secant method) until the calculated current density converges to the set value. This procedure is problematic, since there is no guarantee that the system (with specific flow rates, concentrations and temperatures) can attain the desired current density. A better alternative, would be to specify an external load resistance, R_{ext}, and then match the estimated V_{cell} with the calculated value, $V_{calc}=I_{avg.calc}\times R_{ext}$. This equation can always be fulfilled since it is based on physical behaviors, as opposed to arbitrary guesses. This has not been implemented in this paper, to allow for comparison with results in the literature.

The data used for the simulation is based on the study by Trung and Nguyen (1998), and is presented in Table 1.

The model formulated above constitutes a set of implicit equations, since, as shown in Appendix D, the equations depend nonlinearly on the solid temperature. To reduce the computation time inherent in the implicit formulation, a partially-explicit approximation was developed as an alternative, where the nonlinear expressions of the solid temperature are used explicitly, leading to a linear system for each time step. To compare the difference between the solutions obtained using the original implicit formulation with a partially explicit approximation, the system transient is computed starting from a uniform solid temperature of 343 K using the data from the base case. The evolution of the average temperature and power density with time for varying time-step sizes are presented for both methods in Fig. 2, noting that the system settles well inside 20 s. As can be seen, for a step size of 0.1 s, there is no difference in the results obtained from the two methods. At 0.5 s there is a small difference between the two, with the implicit method repeating the results for time step of 0.1 s. Since the implicit method requires the solution of nonlinear equations, it is more computationally demanding, and, for small step sizes, unnecessary.

The spatial dependence of the variables at the end of the simulation time (i.e. at steady state) can be seen in Fig. 3. The plot shows the computed values indicated by crosses, with a cubic spline used to indicate the continuous profile.

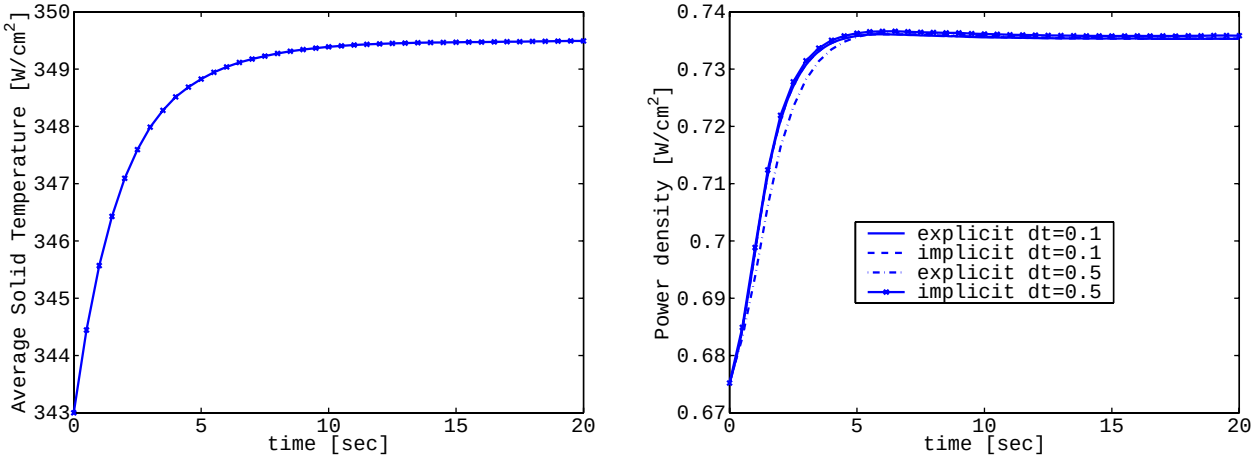

Fig. 2. Simulation of system starting from uniform temperature of 70 °C. The evolution of the average temperature and average power density with time using explicit and implicit Crank–Nicholson for different time steps.

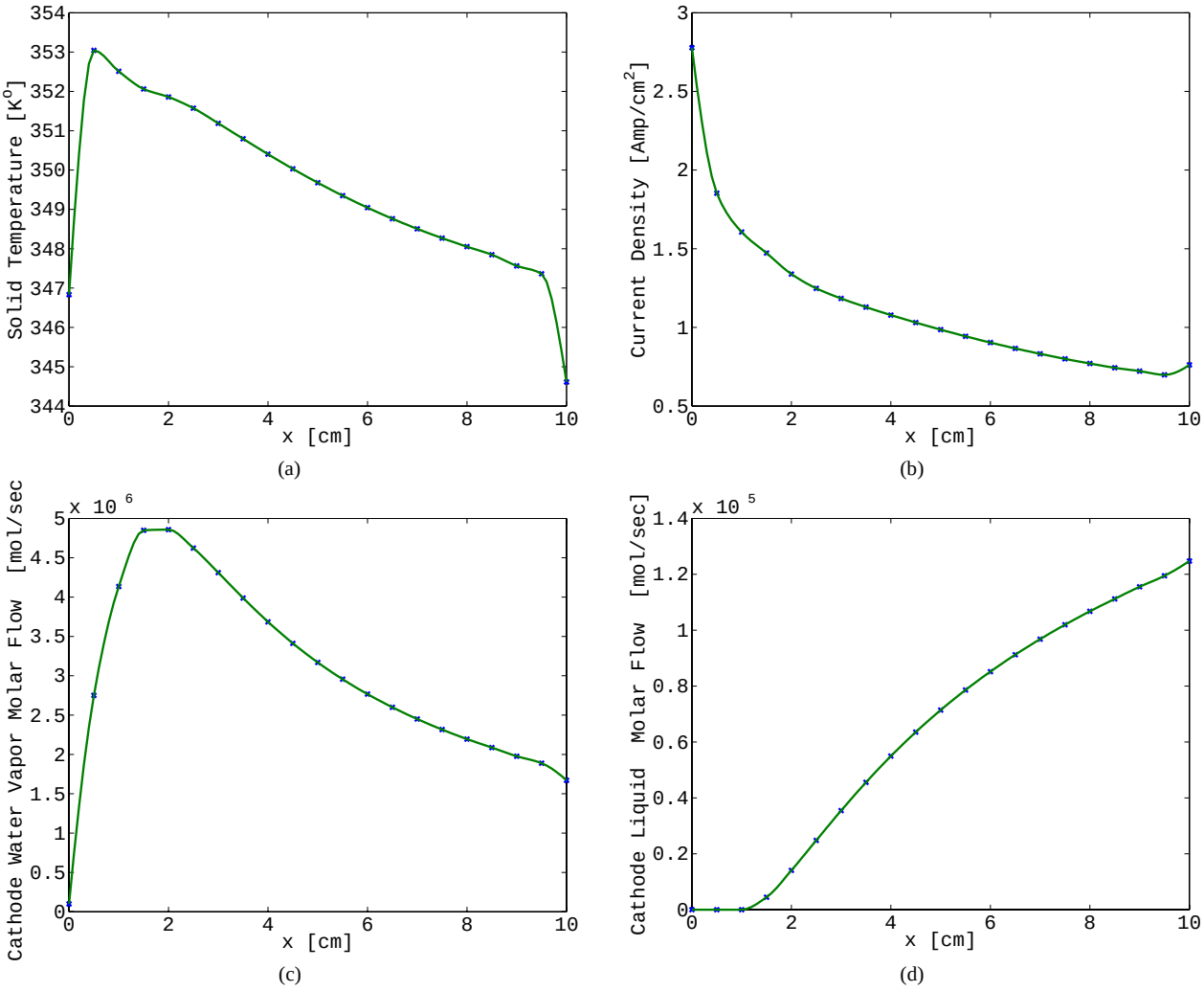

Fig. 3. Spatial dependencies of variables in channel direction: (a) solid temperature; (b) current density; (c) cathode water vapor flow; (d) cathode water liquid flow.

Table 1
Data for base case presented by Trung and Nguyen

Variable	Value
Physical data	
A_{cool} (cm)	0.4
A_g (cm)	0.4
d (cm)	0.1
[a] e (cm)	0.1
[a] f (cm^2)	0.0106
h (cm)	0.1
L (cm)	10
t_m (cm)	0.01275
[a] D_w (cm^2/s)	10^{-6}
[a] D_{O_2} (cm^2/s)	10^{-6}
[a] D_{H_2} (cm^2/s)	10^{-6}
[a] δ (cm)	0.001
$\rho_{m,dry}$ (g/cm^3)	2
[a] ρ_s (g/cm^3)	2
Physical parameters	
I_0 (A/cm^2)	0.01
V_{oc} (V)	1.1
D_0 (cm^2/s)	5.5×10^{-7}
k_c (s^{-1})	100
k_p (cm^2)	1.58×10^{-14}
μ (g/cm s)	3.565×10^{-3}
k_s (W/cm^2K)	0.005
U_c (W/cm^2K)	0.025
U_g (W/cm^2K)	0.025
U_w (W/cm^2K)	0.025
$W_{m,dry}$	1100
ΔH (J/mol)	-2.41×10^5
[a] C_{ps} (J/gK)	1
Operating values for the fuel cell	
$M_{H_2,in}$ (mol/s)	1.14×10^{-5}
$M^v_{w,a,in}$	Saturated
$M^l_{w,a,in}$ (mol/s)	0
$T_{a,in}$ (K)	353
$M_{O_2,in}$ (mol/s)	5.7×10^{-6}
$M^l_{w,a,in}$ (mol/s)	0
$M^v_{w,a,in}$ (mol/s)	0
$T_{c,in}$ (K)	353
P_a (atm)	1
P_c (atm)	1
T_{inf} (K)	343
I_{avg} (A/cm^2)	1.1

[a] Denotes data that were estimated for this paper.

Clearly, the distributed variables feature significant special variation along the channel length.

3. Controllability analysis

To obtain smaller, lighter and cheaper fuel cells, they should be designed to operate at the highest possible power density. In this regard, Fig. 4 displays the power–current relationship for the fuel cell model, operated at constant flowrates of the feed streams. A similar result is obtained when using a constant fuel utilization factor.

To provide guidance for the analysis of the system dynamics and its controllability, a series of step tests were performed on the base case system. These step tests are helpful in determining the influence of various variables on the controlled output. In particular, it is of interest to examine the influence of the cell voltage on the power density, as shown in Fig. 5. Note that the response of the power density to changes in the cell voltage consists of a large initial jump, followed by a gradual change. The initial response is the electrochemical dependence, which is instantaneous, having assumed quasi steady state. The gradual change is due to the slow transient response of the solid temperature profile, which affects the electrochemical behavior along with the quasi-steady-state conditions in the channels. Furthermore, as can be seen in Fig. 5, the response of the power to positive step changes in the cell voltage depends on the operating level selected, with the net change of the power density being either positive at low voltages or negative at high ones.

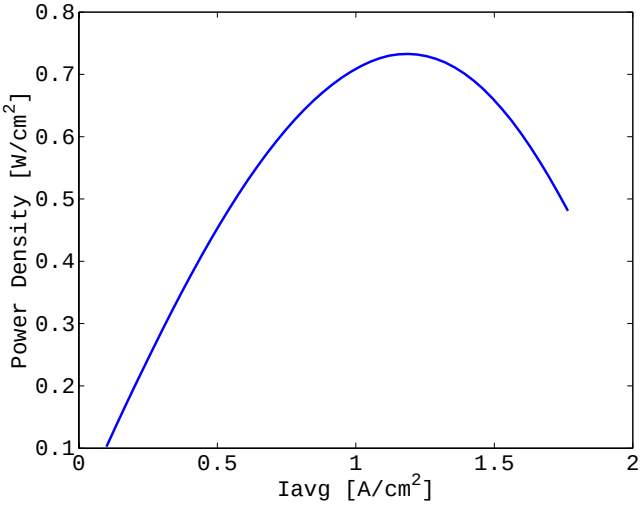

Fig. 4. Power–current curve for base case.

These changes in the static gain ($\Delta P/\Delta V$) are reflected in Fig. 6 where the static gain is plotted as a function of average current density for two sets of conditions: the base case and slightly modified conditions: namely, reactant and oxidant inlet temperatures of 70 and 60 °C, respectively, and a hydrogen and oxygen inlet flowrates of 1.71×10^{-5} and 8.55×10^{-6} mol/s, respectively. As can be seen in Fig. 6, the static gain changes sign for the base case at a current density of about 0.9 A/cm^2. On the other hand, for the modified conditions, the sign change occurs at a higher current density-around 1.3 A/cm^2. Alternatively, if the current density is used as the control variable, the gain between the power density and the average current density ($\Delta P/\Delta I_{avg}$) must be evaluated, as shown in Fig. 7. Once again, a sign change is evident. For the base case, this occurs at roughly 1.1 A/cm^2. Again, for the modified conditions the sign change occurs at a different operating point-about 0.85 A/cm^2. Note that the static gain changes both in magnitude, but more importantly, in sign as well. In addition, other variables change the location of the sign change. This creates severe problems for a control system, since the di-

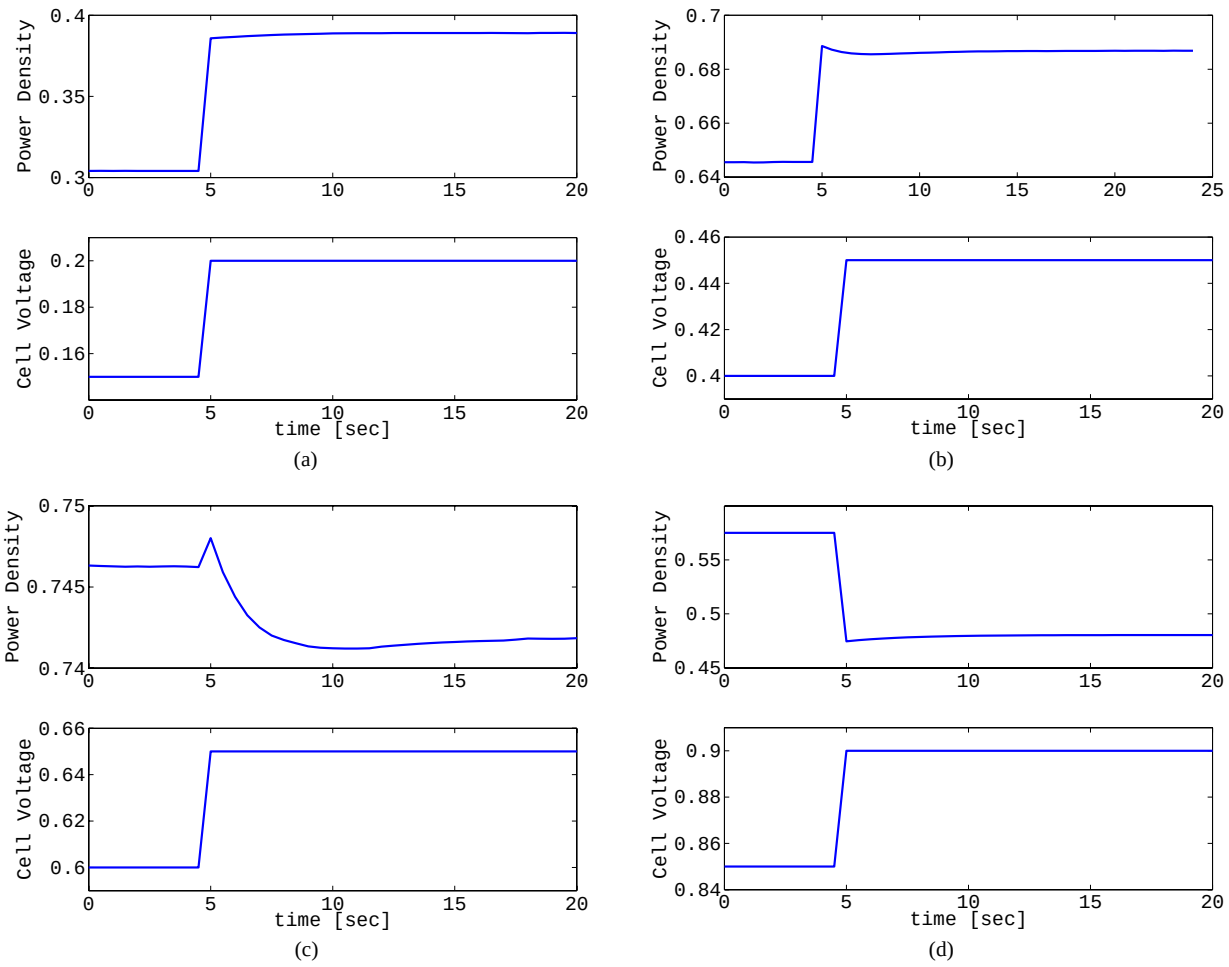

Fig. 5. Step tests for base case. In each case, a step change of 0.05 V is implemented, from operating levels: (a) $V_{cell} = 0.15$ V, (b) $V_{cell} = 0.40$ V, (c) $V_{cell} = 0.60$ V and (d) $V_{cell} = 0.85$ V.

rection of the power's change in response to the control variable (voltage or current density) is not constant and, over a large part of the operating space, difficult to predict accurately. The sign-change in static gain precludes the use of a fixed-gain controller with integral action, since such a controller cannot be stabilized. Two alternative options that can be made to work are adaptive control and nonlinear model-based control.

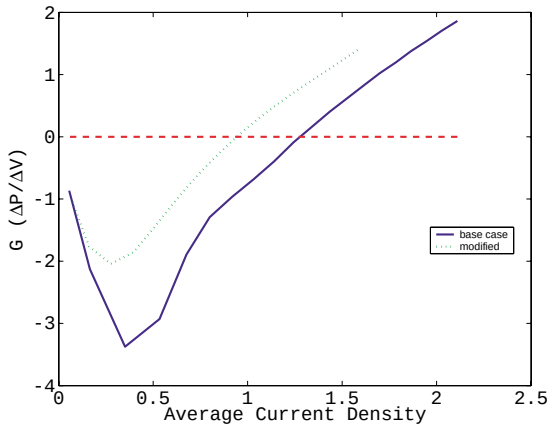

Fig. 6. Static gain of power density to changes in cell voltage for base case and modified conditions.

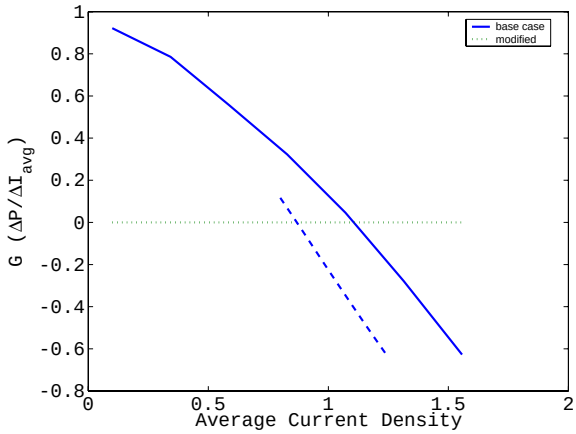

Fig. 7. Static gain of power density to changes in average current density for base case.

A simple adaptive controller attempts to compensate for the changing process gain by adapting itself on the fly. This is difficult to design since the actual behavior of the process is dependent on a number of variables (flowrates, compositions, temperatures, etc.) as demonstrated in Fig. 6. Thus, an adaptive controller that does not account for all of these inputs will experience difficulties, and consequently, will have limited performance and robustness. Alternatively, a fixed-gain controller can be implemented to control the fuel cell in ranges of operating conditions where a sign change in the static gain is not expected. There are two problems with this approach:

1. This kind of system is constantly in danger of straying into the "instability zone," and, once the system gets there, a controller including integral action and previously stable will become unstable when the process gain changes direction.
2. The operating conditions chosen to ensure stable operation are unlikely to be optimal in terms of fuel efficiency and power density.

A control system that relies on a nonlinear model can avoid both problems. The model will indicate the actual influence the control variable will have on the system. This is the motivation to formulate a model that predicts the behavior with sufficient accuracy while being simple enough to enable its use in an on-line optimal control scheme.

3.1. Adaptive control

When designing a control system, a number of requirements need to be satisfied. The control system must eliminate disturbances and track changes in the set point accurately and with sufficient speed. This must be done for as wide a set of conditions as possible. Also, it is desirable that the control system be as simple as possible. Therefore, the design of a simple adaptive controller was attempted first, with the experience serving also as an illustration of some of the phenomena discussed earlier.

Examining Fig. 7 reveals the near linear dependency of the static gain on the current density. Therefore, for control purposes, a standard PI controller could use an adaptive gain inversely proportional to the variable process static gain

$$C(s) = \frac{1}{G(I_{\text{avg}})}\frac{1.5s+1}{1.5s(s+1)}$$
$$G(I_{\text{avg}}) = -1.333I_{\text{avg}} + 1.466 \tag{20}$$

To smooth out the otherwise potentially abrupt changes in the controller gain, the gain value is adjusted using a low pass filter with a time constant of 1 s. Fig. 8 presents the performance obtained with this adaptive controller. Note that it performs nicely for the base case (for which it was designed), converging within roughly 6 s for positive and negative step changes in the power density set point. However, for the modified conditions, it cannot reach the set point of 0.55 W/cm^2 since the controller changes the gain's sign at 1.1 A/cm^2, instead of at 0.85 A/cm^2. Note that the response for the decrease is more aggressive, with overshoot because of the inaccurate value of the static gain that the controller uses. Full design of a standard controller requires that the uncertainty of the actual process gain be addressed.

4. Model predictive control

As has been shown, the fuel cell presents a number of control problems, the most significant of which is the nonlinearity in the vicinity of the peak power density. Furthermore, it is of interest to ensure efficient operation during transients and when extreme load changes are imposed. Consequently, it is proposed to tackle these problems using a nonlinear model predictive control framework.

Model predictive control is part of a family of optimization-based control methods, which are based on on-line

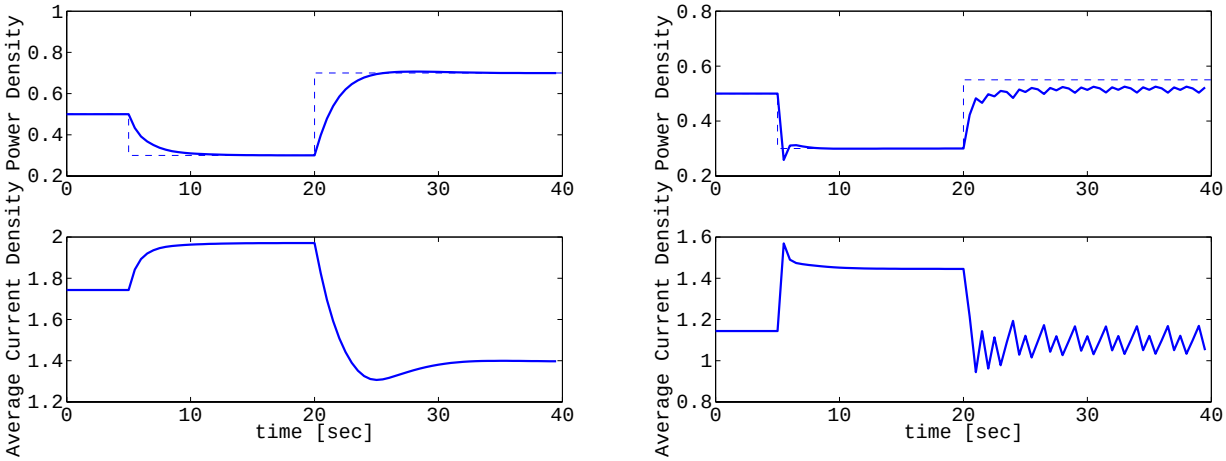

Fig. 8. Control of set point step changes for base case (left) and modified conditions (right).

optimization of future control moves. Using a process model, the optimizer predicts the effect of past inputs on future outputs. Then, using the same model, it computes a sequence of future control moves, such that an objective function, including penalties on the trajectory of predicted tracking error, is minimized. The first of the future control moves is implemented, and the entire optimization is repeated from the next step on, and so on, ad infinitum. Feedback is used to compensate for the model's inaccuracies and to ensure convergence. For a detailed account of nonlinear MPC, the reader is referred to the excellent review by Henson [6].

The definition of the optimization problem offers enormous advantages for advanced control. Typically, the problem formulation includes the satisfaction of the set points for the different output variables (least squared errors). The optimization problem uses a model of the system to predict the output variables values and compares them with the set points. Hence, the performance of the controller is influenced by the accuracy of the model. In addition, the optimization problem commonly includes different degrees of penalty for changes in the control variables. This encourages the controller to avoid excessive changes of the most "expensive" control variables. The advantage of the flexibility of the optimization problem is apparent. Different degrees of importance can be attributed to set point satisfaction, control variable step size and absolute values (influencing stability and controller behavior), and other values of varying importance. For instance, the model's prediction of overall efficiency can be taken into consideration. The optimization can be unconstrained or may include hard constraints (for example safety limits or downstream demands on the process being controlled).

The first step in designing an MPC system is the derivation of a model that the controller will use for the optimization. This model should be as accurate as possible, while being simple enough to allow for repeated calculations during the optimization.

4.1. Reduced model – multiple CSTRs

This simplified model neglects the spatial dependence of the variables in the flow channels. In essence, this assumes CSTR conditions of the reactants and oxidant, and of the coolant, as well. Therefore, differential Eqs. (1)–(8) reduce to the following algebraic equations

$$M_{\mathrm{H_2}} = -\frac{hL}{2F} I_{\mathrm{avg}} + M_{\mathrm{H_2,in}} \tag{21}$$

$$M_{\mathrm{O_2}} = -\frac{hL}{4F} I_{\mathrm{avg}} + M_{\mathrm{O_2,in}} \tag{22}$$

$$M^{\mathrm{l}}_{\mathrm{w},k} = M^{\mathrm{l}}_{\mathrm{w},k,\mathrm{in}} + \frac{k_{\mathrm{c}} hdL}{RT_k} \left\{ \frac{M^{\mathrm{v}}_{\mathrm{w},k}}{\sum_i^{N_k} M_{i,k}} P_k - P^{\mathrm{sat}}_{\mathrm{w}}(T_k) \right\}, \quad k = \mathrm{a}, \mathrm{c} \tag{23}$$

$$M^{\mathrm{v}}_{\mathrm{w,a}} = M^{\mathrm{v}}_{\mathrm{w,a,in}} - \frac{k_{\mathrm{c}} hdL}{RT_{\mathrm{a}}} \left\{ \frac{M^{\mathrm{v}}_{\mathrm{w,a}}}{\sum_i^{N_k} M_{i,\mathrm{a}}} P_{\mathrm{a}} - P^{\mathrm{sat}}_{\mathrm{w}}(T_{\mathrm{a}}) \right\} - \frac{hL\alpha}{F} I_{\mathrm{avg}} \tag{24}$$

$$T_k = T_{k,\mathrm{in}} + \frac{U_{\mathrm{g}} aL(T_{\mathrm{s}} - T_k)}{\sum_i^{N_k} C_{\mathrm{p},i} M_i}, \quad k = \mathrm{a}, \mathrm{c} \tag{25}$$

$$M^{\mathrm{v}}_{\mathrm{w,c}} = M^{\mathrm{v}}_{\mathrm{w,c,in}} - \frac{k_{\mathrm{c}} hdL}{RT_{\mathrm{c}}} \left\{ \frac{M^{\mathrm{v}}_{\mathrm{w,c}}}{\sum_i^{N_k} M_{i,\mathrm{c}}} P_{\mathrm{c}} - P^{\mathrm{sat}}_{\mathrm{w}}(T_{\mathrm{c}}) \right\} + \frac{hL}{F} I_{\mathrm{avg}} \left(\frac{1}{2} + \alpha \right) \tag{26}$$

$$T_{\mathrm{cool}} = T_{\mathrm{cool,in}} + \frac{U_{\mathrm{cool}} bL(T_{\mathrm{s}} - T_{\mathrm{cool}})}{C_{\mathrm{p,w}} M_{\mathrm{cool}}} \tag{27}$$

Similarly, the partial differential Eq. (18) reduces to the ordinary differential equation

$$\rho_{\mathrm{s}} Cp_{\mathrm{s}} \frac{\mathrm{d}T_{\mathrm{s}}}{\mathrm{d}t} = \frac{U_{\mathrm{g}} a}{f}(T_{\mathrm{a}} + T_{\mathrm{c}} - 2T_{\mathrm{s}}) + \frac{U_{\mathrm{cool}} b}{f}(T_{\mathrm{cool}} - T_{\mathrm{s}}) - \frac{e}{f}\left(\frac{\Delta H}{2F} + V_{\mathrm{cell}} \right) I_{\mathrm{avg}} + \frac{1}{fL} \Delta H_{\mathrm{vap}}(T_{\mathrm{s}}) \times (M^{\mathrm{l}}_{\mathrm{w},a} - M^{\mathrm{l}}_{\mathrm{w,a,in}} + M^{\mathrm{l}}_{\mathrm{w,c}} - M^{\mathrm{l}}_{\mathrm{w,c,in}}) - \frac{2U_{\mathrm{inf}}}{L}(T_{\mathrm{s}} - T_{\mathrm{inf}}) \tag{28}$$

The current density is the solution of Eq. (9). The solution method is to solve all the algebraic equations for each time step of the integration of Eq. (28). The solution of α and the current density is cascaded in the following fashion, as shown in Fig. 9:

1. Receive the cell voltage V_{cell}.
2. Guess the cell current density I.
3. Calculate the molar flows of oxygen and hydrogen.
4. Guess α_1.
5. Use the solid temperature to calculate the saturated pressure in the anode and cathode (this simplifies the solution).
6. Calculate the molar flows of the water vapors (see below).
7. Calculate the temperatures of the flow channels.
8. Calculate α and converge (step 4).
9. Calculate the voltage and compare to set voltage
10. Change current accordingly (step 2).

The calculation of the water content in the anode and cathode for a given current density is somewhat tricky. Eqs. (23) and (24) are appropriate if the liquid and vapor in the channel are in equilibrium. This means that liquid water remains in the channel, either by condensation or by only partial

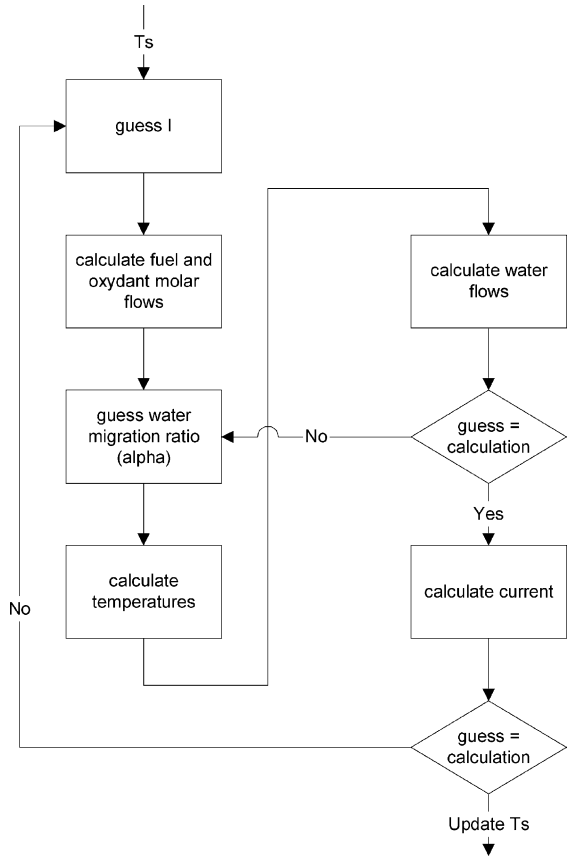

Fig. 9. Flowchart for the solution of the reduced model.

evaporation of feed liquid water. Rearranging Eq. (24) results in the following expression

$$-M_{w,a}^{v2} + \left(\frac{k_c h dL}{RT_s}(P_w^{sat}(T_s) - P_a) + M_{w,a,in}^{v} - M_{H_2} \times -\frac{hL\alpha}{F} I_{avg}\right) M_{w,a}^{v} + \left(\frac{dhk_c L M_{H_2} P_{sat}(T_s)}{RT_s} + M_{H_2} M_{w,a,in}^{v} - \frac{hLM_{H_2}\alpha I_{avg}}{F}\right) = 0 \quad (29)$$

This is easily solved, giving two solutions for the water vapor content. For the solution to be physically meaningful, the solution must be greater than zero and noncomplex. The liquid water is then calculated using Eq. (23). If there is no physical solution for Eq. (29) it means that liquid water is not in equilibrium with the vapor. In other words, the liquid flow out of the channel is zero and the water vapor is the sum of the inlet flow water vapor and liquid water subtracting the water migrating

$$M_{w,a}^{v} = M_{w,a,in}^{v} + M_{w,a,in}^{l} - \frac{hL\alpha}{F} I_{avg}$$
$$M_{w,a}^{l} = 0 \quad (30)$$

If the result of this calculation is negative vapor flow, it means that the guessed values of α and I are not feasible, so for the sake of the calculation, $M_{w,a}^{v}$ is taken as zero. The migrating water is simply the difference between the inlet flows of water (liquid and vapor) and the outlet flows

$$\text{migrate} = M_{w,a,in}^{v} + M_{w,a,in}^{l} - M_{w,a}^{v} - M_{w,a}^{l} \quad (31)$$

This value is then used in the calculation for the water content of the cathode. In a similar fashion to the anode, Eq. (26) is rearranged to give

$$-M_{w,c}^{v2} + \left(M_{w,c,in}^{v} - M_{N_2} - M_{O_2} - \frac{k_c h dL}{RT_s}(P_c - P_w^{sat}(T_s)) + \text{migrate} + \frac{hL}{2F} I_{avg}\right) M_{w,a}^{v} + \left(\frac{k_c h dL}{RT_s} P_w^{sat}(T_s) + M_{w,c,in}^{v} + \text{migrate} + \frac{hL}{2F} I_{avg}\right)(M_{N_2} + M_{O_2}) = 0 \quad (32)$$

whose solution is used in Eq. (23) to calculate the liquid water flow in the cathode. Once again, if neither result of Eq. (32) is physically feasible, the liquid flow is zero, and the vapor flow is calculated using

$$M_{w,a}^{v} = M_{w,a,in}^{v} + M_{w,a,in}^{l} + \text{migrate} + \frac{hL}{2F} I_{avg}$$
$$M_{w,a}^{l} = 0 \quad (33)$$

Note that this includes water vapor generated by the reaction.

At high current densities, there are problems converging the current, since it assumed that there is no pressure drop in the channel. Obviously, if gas molecules are depleted (by reaction and condensation), the pressure will drop, as well. This causes problems since if the total pressure drops, the partial pressures drop, as well. Otherwise, the partial pressures are dependent solely on the *ratios* between the components. Therefore, the partial pressures are calculated using

$$P_i = \frac{M_i}{\sum M_i} P_{tot} \quad (34)$$

Assuming ideal gases, we can use

$$\frac{P_{tot}}{P_{ref}} = \frac{T \sum M_i}{T_{ref} \sum M_{i,ref}} \quad (35)$$

to relate the pressure to the temperature and mole flows in the channel. This results in

$$P_i = \frac{TM_i}{T_{ref} \sum M_{i,ref}} P_{ref} \quad (36)$$

which expresses the dependence of the partial pressures of the components on the mole flows and the temperature in the channels. The reference values are those at the channel inlet.

This model assumes uniform conditions at all points in the channel. If this leads to unsatisfactory accuracy, dividing the system into a number of consecutive CSTRs can incorporate a certain amount of spatial dependence. In this case, the output of one is the input of the next. The assumptions used

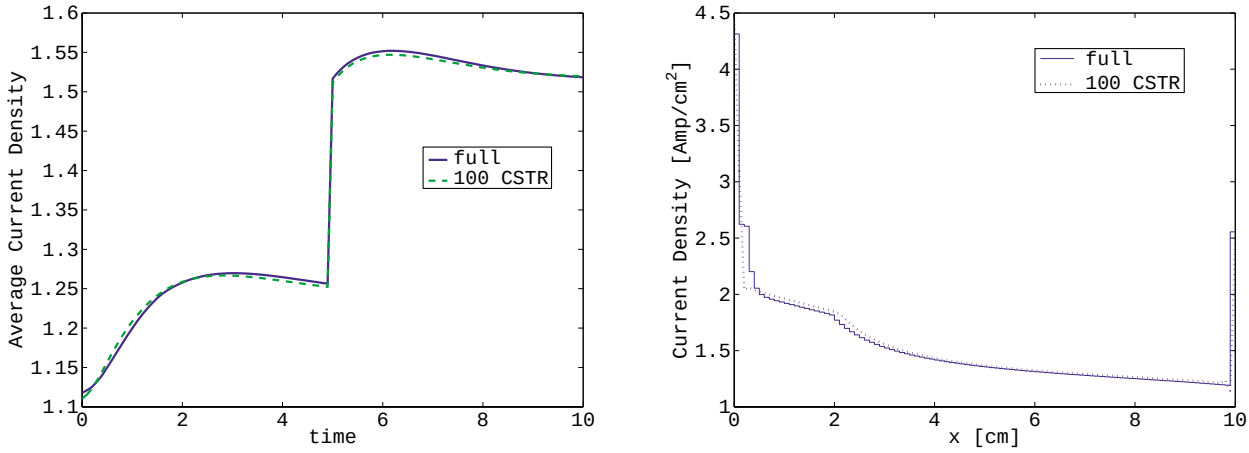

Fig. 10. Comparison of the full model between the multiple CSTR model using 100 CSTRs with no heat conduction – the average current density vs. time and the current density profile at steady state.

in this model are:

1. There is no heat transfer by conduction between two neighboring cells.
2. Heat is only lost to the surroundings from the two outermost CSTRs.
3. The inlet temperatures are used to calculate the saturated pressures and the physical parameters in the channels. This is done because the water flow depends on the channel temperatures (condensation). The current, in turn, depends on the water content, and the temperatures depend on the current. If the inlet temperatures weren't used, the result would be a nonlinear equation.

4.1.1. Results

The following results display the reduced model's ability to predict the behavior of the full-order model. First, it is necessary to ensure that the CSTR model is appropriate by comparing the full model with a large number of CSTRs. We expect that the two models predict identical profiles of the temperatures and concentrations for any given solid temperature profile. When considering the transient behavior over time, it is important to realize that the multiple CSTR model will not agree entirely with the full model, since it does not account for heat exchange by conduction like the full model. The asymptotic case is if the heat transfer by conduction coefficient is zero or negligible. The results of the full model and the multiple CSTR are presented in Fig. 10. As can be seen, the two models are in excellent agreement.

It is important for the model to accurately predict the transient, open loop behavior of a fuel cell under varying conditions, since the performance of a control system relying on this model depends directly on the model's fidelity. Fig. 11 compares open loop response of the system to a step change in the current density from an initial value of 0.5 A/cm^2 to 0.8 A/cm^2 using the full model and the reduced model using varying numbers of CSTRs. Fig. 12 shows the same behavior for a current density step change from 1.1 to 1.4 A/cm^2.

As can be seen, the prediction capabilities of the reduced model are greater at low current densities than at high densities. This makes sense since the spatial dependencies exhibit significantly higher variation at higher values of current

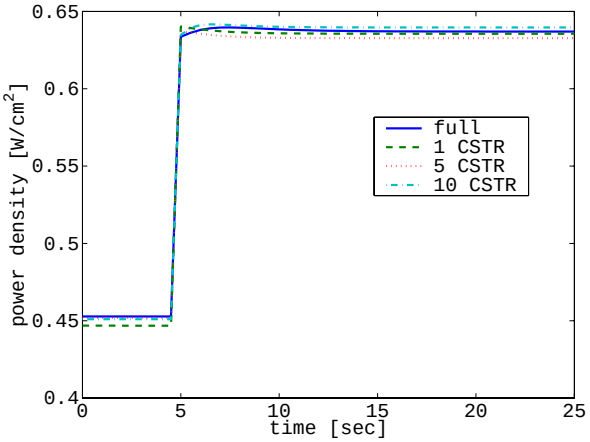

Fig. 11. Open loop response to a step change in the current density from 0.5 to 0.8 A/cm^2.

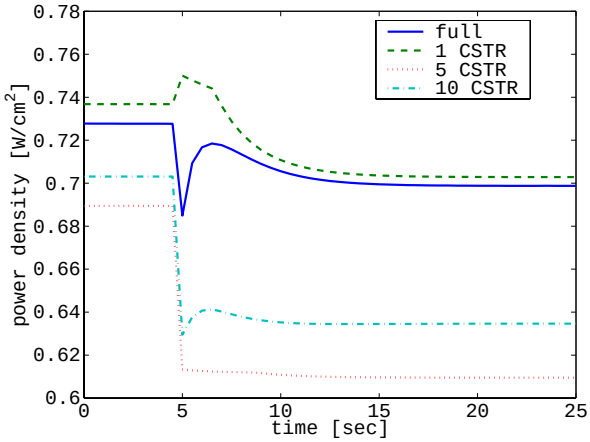

Fig. 12. Open loop response to a step change in the current density from 1.1 to 1.4 A/cm^2.

density, and the reduced model neglects this variation. In Fig. 12, one can see that the 10-CSTR model, while failing to predict the value accurately, still retains the characteristic behavior nicely, whereas the single CSTR model accurately predicts the steady state change in power density. This is important to remember when discussing model-based control, since the quality of the controller depends directly on the quality of the model.

4.2. Amphlett-based reduced model

The solution of the previously mentioned model for a 20 s horizon occupies 2 s of CPU time on a 2.4 GHz computer. This is clearly too slow for practical purposes, since this calculation is at the heart of the MPC objective function. Moreover, there is no way to calculate an analytical gradient for the optimizer forcing the optimizer to calculate one numerically, at each iteration. Therefore, a new method is introduced, based on Amphlett [1], where the current density is set, and the cell voltage is calculated. Amphlett used material and energy balances coupled with a parametric model, which forecasts the electrochemical behavior to model the dynamics of a fuel cell. This paper uses Eqs. (9)–(16) to predict the electrochemical conditions. As the model supports no spatial variation, it is good only for a single CSTR description of a fuel cell.

In this method, the current density is set and the only iterations performed provide the solution of the water content as demonstrated previously. In this formulation, the input variable is the current density, and once the water content is established for that current density, the voltage can be explicitly calculated using Eq. (9).

4.2.1. Results

Fig. 13 demonstrates that the Amphlett-based model is identical to the 1-cell CSTR model. In this example the current density is changed from 0.9 to 1.1 A/cm^2.

As can be seen, the two methods are in complete agreement. This is hardly surprising since the two methods rely on identical equations and assumptions, differing only in numerical approach. Note that Amphlett's approach is significantly faster, but cannot be expanded to more than one CSTR.

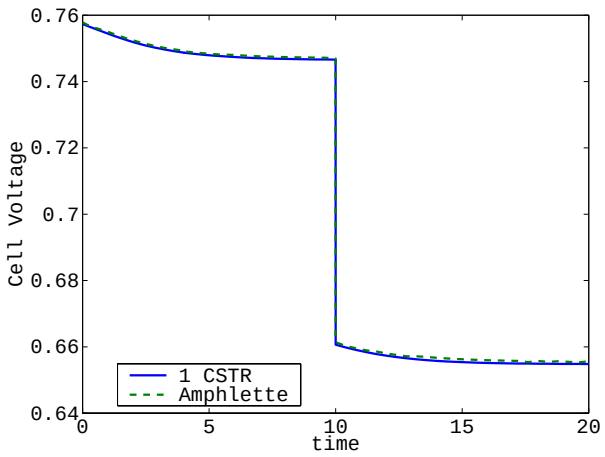

Fig. 13. Comparison of Amphlett based model and 1 CSTR.

4.3. The optimization problem

The objective function for the MPC controller is the minimization of the sum of squared errors between the desired set point and the actual trajectory of the power output, with an additional penalty imposed on rapid changes in the manipulated variables

$$f(u) = \int_0^{t_h} \left[W(t)(P(u,t) - P_{set}(t))^2 + \sum_i S_i(t) \left(\frac{du_i}{dt} \right)^2 \right] dt \quad (37)$$

The weight functions W and S_i are used to increase the importance of specific variables at given instances. For example, the weights may increase over time to ensure rapid convergence with no offset. The function is discretized over time, obtaining the following algebraic function

$$f(u) = (P(u) - P_{set})^T W(P(u) - P_{set}) + \sum_i du_i{}^T S_i du_i \quad (38)$$

The vector $P(u)$ is the actual value of the power density at the different time steps in the prediction horizon, while element i of vector du is the value of u at time step i minus its value at time step $i-1$.

Note that the actual variables in the optimization are the changes in values from each time step to the next. This means that the value of u at time step i is simply the initial value of u plus all the values of du up to time step i.

4.3.1. Results

Fig. 14 shows the performance obtained with MPC for the modified conditions of the base case as in Fig. 8 (using adap-

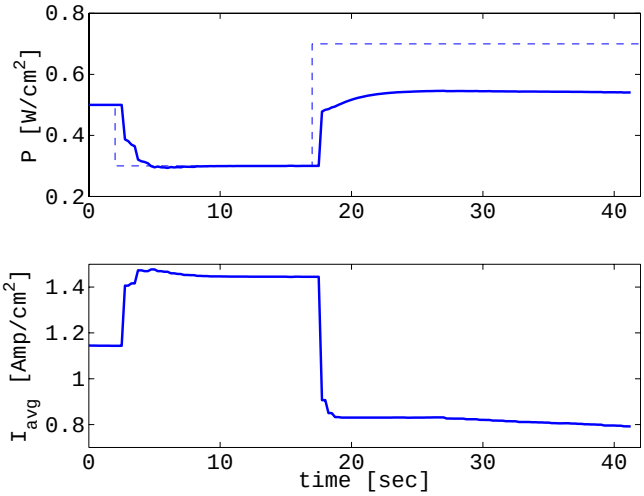

Fig. 14. MPC response for modified conditions of base case.

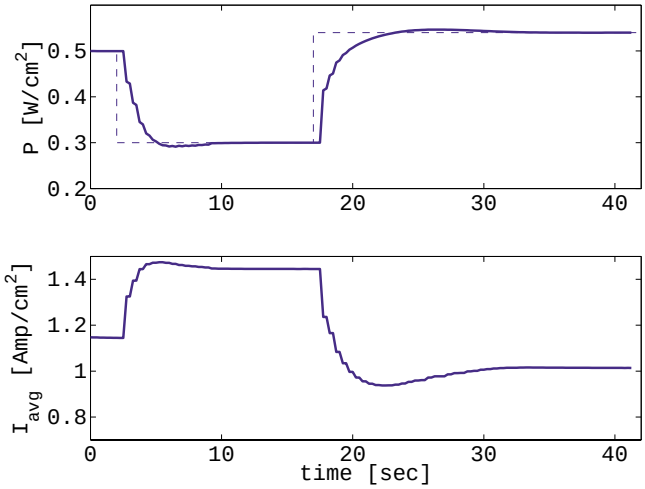

Fig. 15. MPC response for modified conditions of base case to power density of 0.54 W/cm^2.

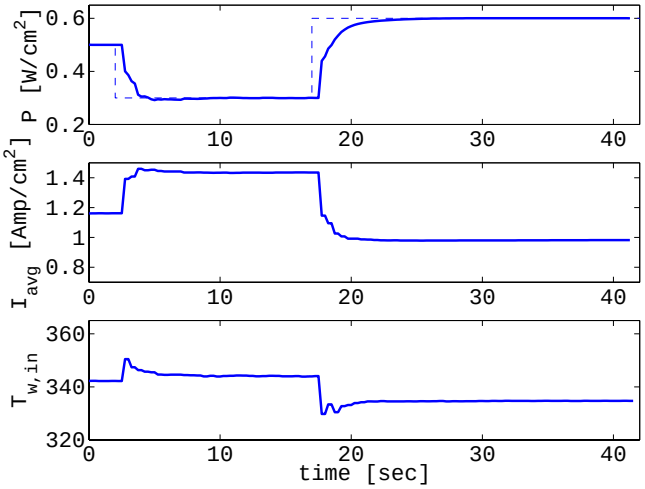

Fig. 17. Multivariable control for $P_{set} = 0.6$ W/cm^2.

tive control). As before, the current density cannot satisfy the increase in power demand, but this time, the controller does not experience loss of stability. Furthermore, the response of MPC in tracking a demand to decrease the power output performs significantly better than the adaptive controller. In Fig. 8, there is a noticeable overshoot because of the process gain uncertainties, whereas the MPC controller drops the power density to the required level in only three seconds, despite the model uncertainties. It is important to note that the observed phase lag in the MPC response in due to the fact that the solution to the MPC optimization problem is only implemented at the next control step. Fig. 15 demonstrates the effectiveness of MPC when operating in the vicinity of the sign change in static gain. Recall that the sign change for the modified conditions occurs at 0.85 A/cm^2. As seen in Fig. 15, the control variable, the current density, crosses that value with no ill effects.

Figs. 16 and 17 demonstrate the multivariable capabilities of MPC. Here, both the current density and the coolant inlet temperature are used as control variables. Fig. 16 shows the performance to the same set point changes as seen in Fig. 15, in which only current density is used. Comparing the results, it can be concluded that the addition of the coolant temperature increases the complexity of the controller without contributing to the performance. On the other hand, Fig. 17 shows that the coolant temperature can be used to enable the system to reach values that would otherwise be out of reach. Fig. 14 shows that the current density alone can not force the system to reach 0.6 W/cm^2, whereas using both variables, as in Fig. 17, the system reaches the set point in five seconds.

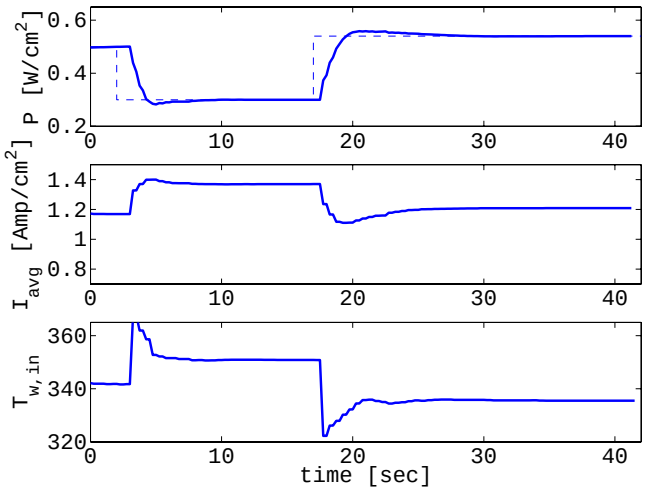

Fig. 16. Multivariable control using the current density and coolant inlet temperature.

5. Conclusions

A detailed model of a fuel cell and its simulation has identified severe nonlinearities in the response to a change in the current density. The sign change of the static gain, which occurs within the normal operating range of the device, together with the uncertainty of the precise location at which this occurs, indicate that nonlinear control is required to adequately regulate the power output of the fuel cell in the case of drastic load changes. Use of nonlinear model predictive control enables accurate control in the case of such uncertainties, with multivariable control improving performance. The use of the MPC algorithm for fuel efficiency while satisfying load-change demands is work in progress.

Acknowledgements

This research was supported by the Israel Science Foundation (Grant no. 25/03-15.4). The support of a Rieger Foundation Scholarship to Josh Golbert for the academic year 2002-3 is acknowledged with thanks.

Appendix A. Derivation of the electrochemical equations

The voltage of the cell as a function of the current density can be evaluated as follows

$$V_{\text{cell}} = V_{\text{oc}} - \eta(x) - \frac{I(x)t_{\text{m}}}{\sigma_{\text{m}}(x)}, \tag{39}$$

where the first term on the right is the open circuit potential. Yi and Nguyen assumed a constant open circuit potential, since their analysis was under isothermal conditions. However, since this equation will be used under transient conditions, the Nernst equation is used to account for temperature and species compositions

$$V_{\text{oc}} = V_{\text{oc}}^0 + \frac{RT}{2F}\ln\left(\frac{P_{\text{H}_2}P_{\text{O}_2}^{0.5}}{P_{\text{H}_2\text{O}}}\right) \tag{40}$$

The second term is the activation overpotential. It is derived from the Butler–Volmer equation [2] for the case where the second expression (anodic) can be neglected (high current densities/overpotentials)

$$I = I_0\left[\frac{C_{\text{O}_2,\text{s}}(x)}{C_{\text{O}_2,\text{b}}(x)}\exp\left(\frac{-\alpha F\eta(x)}{RT}\right) - \frac{C_{\text{H}_2,\text{s}}(x)}{C_{\text{H}_2,\text{b}}(x)}\exp\left(\frac{(1-\alpha)F\eta x}{RT}\right)\right] \tag{41}$$

In fuel cells, the overpotential is mainly at the cathode so the Tafel equation can be used

$$\eta(x) = \frac{RT_{\text{s}}}{0.5\alpha F}\ln\left(\frac{I(x)}{I_0 P_{\text{O}_2}(x)}\right) \approx \frac{RT_{\text{s}}}{F}\ln\left(\frac{I(x)}{I_0 P_{\text{O}_2}(x)}\right), \tag{42}$$

where I^0 is the exchange current density.

Yi and Nguyen used the bulk oxygen partial pressure as the partial pressure at the surface

$$V_{\text{cell}} = V_{\text{oc}}^0 + \frac{RT}{2F}\ln\left(\frac{P_{\text{H}_2}P_{\text{O}_2}^{1/2}}{P_{\text{H}_2\text{O}}}\right) - \frac{RT_{\text{s}}}{F}\ln\left(\frac{I(x)}{I_0 P_{\text{O}_2}(x)}\right) - \frac{I(x)t_{\text{m}}}{\sigma_{\text{m}}(x)} \tag{43}$$

This should be changed, since the concentration overpotential is not taken into account. Assuming constant diffusion coefficient in the gas, D, and a diffusion layer thickness δ, we can say that at steady state conditions the oxygen approaching the surface is equal to the oxygen reacting

$$-D\frac{\text{d}^2 P_{\text{O}_2}}{\text{d}y^2} = 0 \Rightarrow \frac{\text{d}P_{\text{O}_2}}{\text{d}y} = \text{const} \tag{44}$$

However, bulk and surface pressures can be defined. Integrating yields:

$$P_{\text{O}_2}(x, y) = P_{\text{O}_2,\text{s}}(x) + \frac{P_{\text{O}_2}(x,\delta) - P_{\text{O}_2,\text{s}}(x)}{\delta}y \tag{45}$$

and

$$\frac{\text{d}P_{\text{O}_2}(x, y)}{\text{d}y} = \frac{P_{\text{O}_2,\text{b}}(x) - P_{\text{O}_2,\text{s}}(x)}{\delta} \tag{46}$$

Thus, comparing the oxygen approaching and being consumed at the surface

$$-D\frac{P_{\text{O}_2}(x,\delta) - P_{\text{O}_2,\text{s}}(x)}{\delta} = -\frac{I(x)}{4F} \tag{47}$$

and isolating

$$P_{\text{O}_2,\text{s}}(x) = P_{\text{O}_2,\text{b}}(x) - \frac{\delta I(x)}{4FD} \tag{48}$$

In the same fashion

$$P_{\text{H}_2,\text{s}}(x) = P_{\text{H}_2,\text{b}}(x) - \frac{\delta I(x)}{2FD_{\text{H}_2}}$$
$$P_{\text{H}_2\text{O},\text{s}}(x) = P_{\text{H}_2\text{O},\text{b}}(x) + \frac{\delta I(x)}{2FD_{\text{H}_2\text{O}}} \tag{49}$$

This is inserted into Eq. (43) giving

$$V_{\text{cell}} = V_{\text{oc}}^0 + \frac{RT}{2F}\ln\left(\frac{\left[P_{\text{H}_2,\text{b}}(x) - \left(\frac{\delta I(x)}{2FD_{\text{H}_2}}\right)\right]\left[P_{\text{O}_2,\text{b}}(x) - \left(\frac{\delta I(x)}{4FD_{\text{O}_2}}\right)\right]^{0.5}}{P_{\text{H}_2\text{O},\text{b}}(x) + \left(\frac{\delta I(x)}{2FD_{\text{H}_2\text{O}}}\right)}\right) - \frac{RT}{F}\ln\left(\frac{I(x)}{I_0(P_{\text{O}_2,\text{b}}(x) - \left(\frac{\delta I(x)}{4FD_{\text{O}_2}}\right)}\right) - \frac{I(x)t_{\text{m}}}{\sigma_{\text{m}}(x)} \tag{9}$$

It is clear that as the current increases, the cell voltage decreases. The voltage on the electrodes must be constant owing to the high conductivities of the electrodes.

Appendix B. Solution of current density

Eq. (9) is a relatively difficult equation to solve numerically for $I(x)$, since it does not behave nicely at low numbers and negative numbers are not acceptable. Neglecting the concentration overpotential results in an easier expression to solve. Taking an exponent of both sides and rearranging we can define

$$f(I) \equiv \left[\frac{I(x)}{I_0}\right]^2 \exp\left(\left(V_{\text{cell}} - V_{\text{oc}}^0 + \frac{I(x)t_{\text{m}}}{\sigma_{\text{m}}(x)}\right)\frac{2F}{RT}\right) - \frac{P_{\text{H}_2}P_{\text{O}_2}^{5/2}}{P_{\text{H}_2\text{O}}} = 0 \tag{50}$$

Each point along the channel must satisfy this equation. This is a relatively easy function to solve, since its first and second derivatives are unconditionally positive

$$\frac{\mathrm{d}f}{\mathrm{d}I} = 2\frac{1}{I_0}\exp\left(\left(V_{\mathrm{cell}} - V_{\mathrm{oc}}^0 + \frac{I(x)t_{\mathrm{m}}}{\sigma_{\mathrm{m}}(x)}\right)\frac{2F}{RT}\right) \times \left[I(x) + I(x)^2\frac{t_{\mathrm{m}}}{\sigma_{\mathrm{m}}(x)}\frac{F}{RT}\right] \quad (51)$$

This type of function is well-suited to Newton's method, which converges very quickly. In any case the solver backs up Newton's method with bisection iterations.

If the concentration overpotential is not neglected, Eq. (9) is manipulated to give

$$f(I(x)) = \left(P_{\mathrm{H_2,b}}(x) - \frac{\delta I(x)}{2FD_{\mathrm{H_2}}}\right)\left(P_{\mathrm{O_2,b}}(x) - \frac{\delta I(x)}{4FD_{\mathrm{O_2}}}\right)^{2.5} - \frac{I(x)^2}{I_0^2}\left(P_{\mathrm{H_2O,b}}(x) + \frac{\delta I(x)}{2FD_{\mathrm{H_2O}}}\right) \times \exp\left(\left(V_{\mathrm{cell}} - V_{\mathrm{oc}}^0 + \frac{I(x)t_{\mathrm{m}}}{\sigma_{\mathrm{m}}(x)}\right)\frac{2F}{RT}\right) = 0 \quad (53)$$

whose first derivative

$$\frac{\mathrm{d}f}{\mathrm{d}I} = -\frac{I(x)^2\delta\exp(2F/RT(V_{\mathrm{cell}} - V_{\mathrm{oc}}^0 + (I(x)t_{\mathrm{m}}/\sigma_{\mathrm{m}}(x))))}{2D_{\mathrm{H_2O}}FI_0^2} - \frac{2I(x)\exp(2F/RT(V_{\mathrm{cell}} - V_{\mathrm{oc}}^0 + (I(x)t_{\mathrm{m}}/\sigma_{\mathrm{m}}(x))))\,(P_{\mathrm{H_2O,b}}(x) + (\delta I(x)/2FD_{\mathrm{H_2O}}))}{I_0^2} - \frac{0.625\delta(P_{\mathrm{H_2},b}(x) - (\delta I(x)/2FD_{\mathrm{H_2}}))(P_{\mathrm{O_2,b}}(x) - (\delta I(x)/4FD_{\mathrm{O_2}}))^{1.5}}{D_{\mathrm{O_2}}F} - \frac{\delta(P_{\mathrm{O_2,b}}(x) - (\delta I(x)/4FD_{\mathrm{O_2}}))^{2.5}}{2D_{\mathrm{H_2}}F} - \frac{2I(x)^2\exp(2F/RT(V_{\mathrm{cell}} - V_{\mathrm{oc}}^0 + (I(x)t_{\mathrm{m}}/\sigma_{\mathrm{m}}(x))))\,Ft_{\mathrm{m}}(P_{\mathrm{H_2O,b}}(x) + (\delta I(x)/2FD_{\mathrm{H_2O}}))}{I_0{}^2RT\sigma_{\mathrm{m}}(x)} \quad (54)$$

is unconditionally negative. The second derivative, however, may change signs, which can be problematic for Newton's method of solution. Consequently, Newton's method may experience convergence problems, depending on the values in the equation, and should be protected using bisection iterations.

As said before, this value of $I(x)$ is used in the ODEs. Since the membrane conductivity, σ, temperatures and concentrations change along the channel, the local current density will vary, as well. Note that since all the changes are continuous, the previous solution for $I(x)$ is an excellent initial guess for $I(x + \mathrm{d}x)$.

Appendix C. Resolving problems when integrating along the channel

As stated in Section 2, numerical solution of the system equations presents several challenges. Firstly, the system equations as formulated depend on whether or not liquid water is present in the channel. Obviously, if liquid water is not present there can be no evaporation regardless of the vapor partial pressure. The simple solution of adding a logical switching condition introduces stiffness to the ODEs being solved, which can easily lead to unstable or oscillatory numerical solutions. Instead, the ODE solver implemented uses MATLAB's "events" option, which checks for a number of situations:

1. Cathode or anode liquid reaches zero.
2. Cathode or anode vapor partial pressure reaches its saturated pressure.

In each case, the ODE solver terminates the integration, returning the calculations up to that point and restarts calculation with a different set of ODEs. For example, if there is no liquid water in the cathode and the vapor pressure is below saturation, Eq. (3) is not used. When the cathode becomes saturated, the integration terminates and is restarted from the same point, this time using Eq. (3).

In addition, it is noted that the system of equations involves variables with scales of several orders of magnitude apart-namely, the temperatures are in K of o(10^2) while molar flow rates are in mol/s of o(10^{-6}), which again leads to problems in their numerical solution. This is resolved by scaling all molar flowrates using the value of the inlet molar flow of hydrogen, and all temperatures using the temperature of the solid at $x = 0$, for example

$$M_{\mathrm{H_2}}(x) = M_{\mathrm{H_2}}(0)M_{\mathrm{H_2,scaled}}(x)$$
$$T_{\mathrm{a}}(x) = T_{\mathrm{s}}(0)T_{\mathrm{a,scaled}}(x)$$

The ODEs used in the actual integration are modified to use the scaled variables.

Appendix D. Solution of transient PDE

The transient PDE describing the temperature profile of the solid in the channel direction (Eq. (18)) is solved using the Crank-Nicholson method. This method approximates the partial differentials by finite differences, resulting in a system of algebraic equations, which describe the dependence of the temperature profile at time $j + 1$ on the profile at time j. This system is solved starting at the initial conditions, with each solution giving the temperature profile at the next time step.

Introducing the following expressions

$$Y = \beta_1(T_{\mathrm{a}} + T_{\mathrm{c}}) + \beta_2 T_{\mathrm{w}}$$
$$M = M^1_{\mathrm{w,a,i+1}} - M^1_{\mathrm{w,a,i-1}} + M^1_{\mathrm{w,c,i+1}} - M^1_{\mathrm{w,c,i-1}} \quad (55)$$

Eq. (17) becomes

$$\frac{T_{\mathrm{s,i,j+1}} - T_{\mathrm{s,i,j}}}{\Delta t} = \alpha \frac{T_{\mathrm{s,i+1,j+1/2}} - 2T_{\mathrm{s,i,j+1/2}} + T_{\mathrm{s,i-1,j+1/2}}}{\Delta x^2} + Y_{\mathrm{i,j+1/2}} - \gamma T_{\mathrm{s,i,j+1/2}} - \varepsilon \left(\frac{\Delta H}{2F} + V_{\mathrm{cell}} \right) \times I_{\mathrm{i,j+1/2}} + \frac{\phi}{2\Delta x} \Delta H_{\mathrm{vap}}(T_{\mathrm{i,j+1/2}}) M_{\mathrm{i,j+1/2}} \tag{56}$$

Inserting expressions for the solutions on the "half-way point" in terms of values on the solution grid

$$T_{\mathrm{s},i+1,j+1/2} \approx \frac{T_{\mathrm{s},i+1,j+1} + T_{\mathrm{s},i+1,j}}{2}, \quad T_{\mathrm{s},i,j+1/2} \approx \frac{T_{\mathrm{s},i,j+1} + T_{\mathrm{s},i,j}}{2}, \quad T_{\mathrm{s},i-1,j+1/2} \approx \frac{T_{\mathrm{s},i-1,j+1} + T_{\mathrm{s},i-1,j}}{2}, \tag{57}$$

and rearranging gives

$$-\alpha T_{\mathrm{s},i+1,j+1} + \left(\frac{2\Delta x^2}{\Delta t} + 2\alpha + \gamma \Delta x^2 \right) T_{\mathrm{s},i,j+1} - \alpha T_{\mathrm{s},i-1,j+1} = \alpha T_{\mathrm{s},i+1,j} + \left(\frac{2\Delta x^2}{\Delta t} - 2\alpha - \gamma \Delta x^2 \right) T_{\mathrm{s},i,j} + \alpha T_{\mathrm{s},i-1,j} + 2\Delta x^2 Y_{i,j+1/2} - 2\Delta x^2 \varepsilon \left(\frac{\Delta H}{2F} + V_{\mathrm{cell}} \right) \times I_{i,j+1/2} + \phi \Delta x \Delta H_{\mathrm{vap}}(T_{i,j+1/2}) M_{i,j+1/2} \tag{58}$$

Recall that Y and I are calculations based on T_{s}. Solving this entire system implicitly requires iterations of guessing the profile of T_{s} at time $j+1$, calculating Y and I at time $j+1$, and inserting them into the equation. The right hand side will then be a vector, and the linear system can be solved resulting in a calculated profile for T_{s}. The guess for T_{s} can then be iteratively updated, until the solution for T_{s} at time $j+1$ converges.

Alternatively, Y and I can be used explicitly, in which case the linear system can be solved immediately. In this case, a small step size should be used, to ensure stability. Discretizing Eq. (19) for the edges and rearranging gives

$$\begin{aligned} -(3k + 2\Delta x U_c) T_{\mathrm{s},1,j+1} + 4k T_{\mathrm{s},2,j+1} - k T_{\mathrm{s},3,j+1} &= -2\Delta x U_c T_{\mathrm{inf}} \\ k T_{\mathrm{s},n-2,j+1} - 4k T_{\mathrm{s},n-1,j+1} + (3k + 2\Delta x U_c) T_{\mathrm{s},n,j+1} &= 2\Delta x U_c T_{\mathrm{inf}} \end{aligned} \tag{59}$$

Arranging all the equations into matrix form and defining matrices A and B, and vector C:

$$\underline{\underline{A}} = \begin{bmatrix} -(3k + 2\Delta x U_c) & 4k & -k & 0 & \cdots & 0 \\ \ddots & \ddots & \ddots & 0 & \cdots & 0 \\ 0 & -\alpha & \dfrac{2\Delta x^2}{\Delta t} + 2\alpha + \gamma \Delta x^2 & -\alpha & 0 & \vdots \\ \vdots & \ddots & \ddots & \ddots & \ddots & \vdots \\ 0 & \ddots & \ddots & \ddots & \ddots & \ddots \\ 0 & \cdots & 0 & k & -4k & 3k + 2\Delta x U_c \end{bmatrix} \tag{60}$$

$$\underline{\underline{B}} = \begin{bmatrix} 0 & 0 & 0 & 0 & \cdots & 0 \\ \alpha & \ddots & \alpha & 0 & \cdots & 0 \\ 0 & \alpha & \left(\dfrac{2\Delta x^2}{\Delta t} - 2\alpha - \gamma \Delta x^2 \right) & \alpha & 0 & \vdots \\ \vdots & \ddots & \ddots & \ddots & \ddots & \vdots \\ 0 & \ddots & \ddots & \alpha & \ddots & \alpha \\ 0 & \cdots & 0 & 0 & 0 & 0 \end{bmatrix} \tag{61}$$

$$\underline{C} = 2\Delta x^2 \begin{bmatrix} 0 \\ Y_{2,j} \\ \vdots \\ Y_{n-1,j} \\ 0 \end{bmatrix} - 2\Delta x^2 \varepsilon \left(\frac{\Delta H}{2F} + V_{\mathrm{cell}} \right) \begin{bmatrix} 0 \\ I_{2,j} \\ \vdots \\ I_{n-1,j} \\ 0 \end{bmatrix} + \begin{bmatrix} -2\Delta x U_c T_{\mathrm{inf}} \\ 0 \\ \vdots \\ 0 \\ 2\Delta x U_c T_{\mathrm{inf}} \end{bmatrix} + \phi \Delta x \begin{bmatrix} 0 \\ \Delta H_{\mathrm{vap}}(T_{2,j}) M_{2,j} \\ \vdots \\ \Delta H_{\mathrm{vap}}(T_{n-1,j}) M_{n-1,j} \\ 0 \end{bmatrix} \tag{62}$$

The linear system can then be written as

$$\underline{\underline{A}}\,\underline{T_{j+1}} = \underline{\underline{B}}\,\underline{T_j} + \underline{C} \tag{63}$$

Note that matrices $\underline{\underline{A}}$ and $\underline{\underline{B}}$ remain constant for all times and only $\underline{C}$ needs to be updated from time step to time step.

If the system is to be integrated implicitly, Eq. (58) becomes

$$\begin{aligned}
&-\alpha T_{\mathrm{s},i+1,j+1} + \left(\frac{2\Delta x^2}{\Delta t} + 2\alpha + \gamma\Delta x^2\right) T_{\mathrm{s},i,j+1} - \alpha T_{\mathrm{s},i-1,j+1} \\
&= \alpha T_{\mathrm{s},i+1,j} + \left(\frac{2\Delta x^2}{\Delta t} - 2\alpha - \gamma\Delta x^2\right) T_{\mathrm{s},i,j} \\
&+ \alpha T_{\mathrm{s},i-1,j} + \Delta x^2 Y_{i,j+1} + \Delta x^2 Y_{i,j} - \Delta x^2 \varepsilon \\
&\times \left(\frac{\Delta H}{2F} + V_{\mathrm{cell}}\right) I_{i,j+1} - \Delta x^2 \varepsilon \left(\frac{\Delta H}{2F} + V_{\mathrm{cell}}\right) I_{i,j} \\
&+ \frac{\phi\Delta x}{2} \Delta H_{\mathrm{vap}}(T_{i,j+1}) M_{i,j+1} + \frac{\phi\Delta x}{2} \Delta H_{\mathrm{vap}}(T_{i,j}) M_{i,j}
\end{aligned} \tag{64}$$

In which case

$$\begin{aligned}
\underline{C} = \Delta x^2 &\begin{bmatrix} 0 \\ Y_{2,j} \\ \vdots \\ Y_{n-1,j} \\ 0 \end{bmatrix} - \Delta x^2 \varepsilon \left(\frac{\Delta H}{2F} + V_{\mathrm{cell}}\right) \begin{bmatrix} 0 \\ I_{2,j} \\ \vdots \\ I_{n-1,j} \\ 0 \end{bmatrix} \\
&+ \begin{bmatrix} -2\Delta x U_c T_{\mathrm{inf}} \\ 0 \\ \vdots \\ 0 \\ 2\Delta x U_c T_{\mathrm{inf}} \end{bmatrix} + \frac{\phi\Delta x}{2} \begin{bmatrix} 0 \\ \Delta H_{\mathrm{vap}}(T_{2,j}) M_{2,j} \\ \vdots \\ \Delta H_{\mathrm{vap}}(T_{n-1,j}) M_{n-1,j} \\ 0 \end{bmatrix}
\end{aligned} \tag{65}$$

$$\begin{aligned}
\underline{D}(\underline{T_{j+1}}) \equiv \Delta x^2 &\begin{bmatrix} 0 \\ Y_{2,j+1} \\ \vdots \\ Y_{n-1,j+1} \\ 0 \end{bmatrix} - \Delta x^2 \varepsilon \left(\frac{\Delta H}{2F} + V_{\mathrm{cell}}\right) \\
&\times \begin{bmatrix} 0 \\ I_{2,j+1} \\ \vdots \\ I_{n-1,j+1} \\ 0 \end{bmatrix} + \begin{bmatrix} -2\Delta x U_c T_{\mathrm{inf}} \\ 0 \\ \vdots \\ 0 \\ 2\Delta x U_c T_{\mathrm{inf}} \end{bmatrix}
\end{aligned}$$

$$+ \frac{\phi\Delta x}{2} \begin{bmatrix} 0 \\ \Delta H_{\mathrm{vap}}(T_{i,j+1}) M_{i,j+1} \\ \vdots \\ \Delta H_{\mathrm{vap}}(T_{i,j+1}) M_{i,j+1} \\ 0 \end{bmatrix} \tag{66}$$

The nonlinear set of equations is

$$\underline{\underline{A}}\,\underline{T_{\mathrm{s},j+1}} + \underline{\underline{D}}(\underline{T_{\mathrm{s},j+1}}) = \underline{\underline{B}}\,\underline{T_{\mathrm{s},j}} + \underline{C}(\underline{T_{\mathrm{s},j}}) \tag{67}$$

This is solved using a relaxed successive substitution method where

$$\underline{T_{\mathrm{s},j+1}} = f(\underline{T_{\mathrm{s},j+1}}) = \underline{\underline{A}}^{-1}(\underline{\underline{B}}\,\underline{T_{\mathrm{s},j}} + \underline{C}(\underline{T_{\mathrm{s},j}}) - \underline{\underline{D}}(\underline{T_{\mathrm{s},j+1}})) \tag{68}$$

This can be accelerated or damped using Wegstein's method.

References

[1] J.C. Amphlett, R.F. Mann, B.A. Peppley, P.R. Roberge, A. Rodrigues, A model predicting transient responses of proton exchange membrane fuel cells, J. Power Sources 61 (1996) 183–188.

[2] A.J. Bard, L.R. Faulkner, Electrochemical Methods-Fundamentals and Applications, John Wiley and Sons, Inc., New York, 2001.

[3] C. Berger, Handbook of Fuel Cell Technology, Prentice-Hall, Inc., Englewood Cliffs, NJ, 1968.

[4] P. Costamagna, Transport phenomena in polymeric membrane fuel cells, Chem. Eng. Sci. 56 (2001) 323–332.

[5] T.F. Fuller, J. Newman, Water and thermal management in solid–polymer–electrolyte fuel cells, J. Electrochem. Soc. 140 (5) (1993) 1218–1225.

[6] M.A. Henson, Nonlinear model predictive control: current status and future directions, Comput. Chem. Eng. 23 (2) (1998) 187–202.

[7] B. Kang, J. Koh, H. Chun Lim, Experimental study on the dynamic characteristics of kW-scale molten carbonate fuel cell systems, J. Power Sources 94 (2001) 51–62.

[8] J.H. Lee, T.R. Lalk, Modeling fuel cell stack systems, J. Power Sources 73 (1998) 229–241.

[9] J.T. Pukrushpan, A.G. Stefanopoulou, H. Peng, Modeling and Control for PEM Fuel Cell Stack System, Proceedings of the American Control Conference, Anchorage, Alaska, May 8–10, 2002.

[10] T. Schultz, S. Zhou, K. Sundmacher, Current status of and recent developments in the direct methanol fuel cell, Chem. Eng. Technol. 24 (12) (2001) 1223–1233.

[11] T.E. Springer, T.A. Zawodzinski, Polymer electrolyte fuel cell model, J. Electrochem. Soc. 138 (8) (1991) 2334–2342.

[12] J.S. Yi, T.V. Nguyen, An along-the-channel model for proton exchange membrane fuel cells, J. Electrochem. Soc. 145 (4) (1998) 1149–1159.